arXiv:1607.00371v1 [hep-ex] 1 Jul 2016

Measurement of the $e^+e^- \to \omega\eta$ cross section below $\sqrt{s} = 2$ GeV

M. N. Achasov,[1,2] A. Yu. Barnyakov,[1,2] K. I. Beloborodov,[1,2] A. V. Berdyugin,[1,2]
A. G. Bogdanchikov,[1] A. A. Botov,[1,*] T. V. Dimova,[1,2] V. P. Druzhinin,[1,2]
V. B. Golubev,[1,2] L. V. Kardapoltsev,[1,2] A. S. Kasaev,[1] A. G. Kharlamov,[1,2]
A. N. Kirpotin,[1] D. P. Kovrizhin,[1,2] I. A. Koop,[1,2,3] A. A. Korol,[1,2]
S. V. Koshuba,[1,2] A. S. Kupich,[1,2] K. A. Martin,[1] N. A. Melnikova,[1]
A. E. Obrazovsky,[1] E. V. Pakhtusova,[1] A. I. Senchenko,[1] S. I. Serednyakov,[1,2]
Z. K. Silagadze,[1,2] Yu. M. Shatunov,[1,2] D. A. Shtol,[1,2] D. B. Shwartz,[1,2]
A. N. Skrinsky,[1] I. K. Surin,[1,2] Yu. A. Tikhonov,[1,2] and A. V. Vasiljev[1,2]

[1]*Budker Institute of Nuclear Physics, SB RAS, Novosibirsk 630090, Russia*

[2]*Novosibirsk State University, Novosibirsk 630090, Russia*

[3]*Novosibirsk State Technical University, Novosibirsk 630092, Russia*

The cross section for the process $e^+e^- \to \omega\eta$ is measured in the center-of-mass energy range 1.34–2.00 GeV. The analysis is based on data collected with the SND detector at the VEPP-2000 e^+e^- collider. The measured $e^+e^- \to \omega\eta$ cross section is the most accurate to date. A significant discrepancy is observed between our data and previous BABAR measurement.

PACS numbers: 13.66.Bc, 14.40.Cs, 14.40.Aq, 13.40.Gp

I. INTRODUCTION

The main goal of experiments with the SND detector [1] at the e^+e^- collider VEPP-2000 [2] is a precision measurement of the total cross section of e^+e^- annihilation to the hadrons in the center-of-mass (c.m.) energy region $E = \sqrt{s} < 2$ GeV. The total cross section is necessary for calculation of the running electromagnetic coupling constant and the muon anomalous magnetic moment. Below 2 GeV the total hadronic cross section is calculated as a sum of exclusive cross sections for all possible hadronic modes. For some

*e-mail: A.A.Botov@inp.nsk.su

of them, e.g., $\pi^+\pi^-\pi^0\eta$, $\pi^+\pi^-\pi^0\pi^0\pi^0$, $\pi^+\pi^-\pi^0\pi^0\eta$, which may give a sizable contribution to the total hadronic cross section, experimental information is scarce or absent. The process $e^+e^- \to \pi^+\pi^-\pi^0\eta$ can proceed through the $\omega\eta$, $\phi\eta$ intermediate states, the cross sections for which are already measured [3–5], and also through other states, e.g., $\rho a_0(980)$. This work is dedicated to the measurement of the $e^+e^- \to \omega\eta$ cross section. We analyze the $\pi^+\pi^-\pi^0\eta$ final state with η meson decayed to $\gamma\gamma$. The methods developed for the selection of $e^+e^- \to \omega\eta \to \pi^+\pi^-\pi^0\eta$ events will be used in future detailed study of the process $e^+e^- \to \pi^+\pi^-\pi^0\eta$ and measurement its total cross section.

Previously, the process $e^+e^- \to \omega\eta$ was measured using the ISR technique in the BABAR experiment [3] in the six pion final state.

II. DETECTOR AND EXPERIMENT

SND [1] is a general purpose nonmagnetic detector. Its main part is a spherical three-layer electromagnetic calorimeter with 560 individual NaI(Tl) crystals per layer. The calorimeter covers a solid angle of 95% of 4π and has a width of $13.4X_0$, where X_0 is a radiative length. The calorimeter energy resolution for photons is $\sigma_E/E_\gamma = 4.2\%/\sqrt[4]{E_\gamma(\mathrm{GeV})}$. The angular resolution is about 1.5°. Inside the calorimeter, around the collider beam pipe, a tracking system is located, which consists of a nine-layer drift chamber and a proportional chamber with cathode-strip readout in a common gas volume. The tracking system covers a solid angle of 94% of 4π. Its angular resolution is 0.45° in the azimuthal angle and 0.8° in the polar angle. A system of aerogel Cherenkov counters located between the tracking system and the calorimeter is used for charged kaon identification. Outside the calorimeter, a muon detector consisting of proportional tubes and scintillation counters is placed.

The analysis is based on data with an integrated luminosity of 27 pb^{-1} recorded with the SND detector in 2011–2012 in 36 energy points above the threshold of the process under study.

During the experiment, the beam energy was determined using measurements of the magnetic filed in the collider bending magnets. To fix the absolute energy scale, a scan of the $\phi(1020)$ resonance was performed and its mass was measured. In 2012 the beam energy was measured in several energy points near 2 GeV by the back-scattering-laser-light system [6, 7]. The absolute energy measurements were used for calibration of the momentum measurement

in the CMD-3 detector, which collected data at VEPP-2000 simultaneously with SND. The absolute c.m. energies for all scan points were then determined using average momentum in Bhabha and $e^+e^- \to p\bar{p}$ events with accuracy of 2–6 MeV [8]. Because of the absence of any narrow structures in the $e^+e^- \to \omega\eta$ cross section, the 36 energy points are merged into 13 energy intervals listed in Table I. For each interval the weighted average value of the c.m. energy ($\overline{E}_i$) is also listed, which is calculated as $\sum E_j L_j \sigma_{vis}(E_j) / \sum L_j \sigma_{vis}(E_j)$, where the sum is over the scan energy points included into the i-th interval, L_j is the integrated luminosity for the j-th scan point, and σ_{vis} is the visible cross section for $e^+e^- \to \omega\eta$ defined in Sec. VII.

Simulation of the signal and background processes is done with Monte Carlo (MC) event generators. The generators take into account radiative corrections to the initial particles calculated according to Ref. [9]. The angular distribution of additional photons radiated by the initial electron and positron is simulated according to Ref. [10]. The cross-section energy dependences needed for radiative-correction calculation are taken from existing data, e.g., from Ref. [3] for the process $e^+e^- \to \omega\eta$.

Interactions of the generated particles with the detector materials are simulated using GEANT4 software [11]. The simulation takes into account variation of experimental conditions during data taking, in particular dead detector channels and beam-induced background. The beam background leads to appearance of spurious photons and charged particles in detected events. To take this effect into account, simulation uses special background events recorded during data taking with a random trigger, which are superimposed on simulated events.

III. LUMINOSITY MEASUREMENT

The process of Bhabha scattering $e^+e^- \to e^+e^-$ is used for luminosity measurement. Bhabha events are selected with the following conditions. They must contain at least two charged particles originated from the beam interaction region. The particle energies are determined on their energy depositions in the calorimeter. Further conditions are applied to the two most energetic charged particles. Their energies must be greater than $0.6E_{beam}$, where E_{beam} is the beam energy, and their polar ($\theta_{1,2}$) and azimuthal ($\phi_{1,2}$) angles must satisfy the conditions $(180^\circ - |\theta_1 - \theta_2|)/2 > 50^\circ$, $|\theta_1 + \theta_2 - 180^\circ| < 15^\circ$, $||\phi_1 - \phi_2| - 180^\circ| < 10^\circ$.

The detection efficiency and cross section for Bhabha events are determined using the event generator BHWIDE [12]. The integrated luminosity measured for each energy interval is listed in Table I. The theoretical uncertainty of the luminosity measurement is less than 0.5%. The systematic uncertainty on the detection efficiency is estimated by variation of the selection criteria used and does not exceed 2%.

IV. EVENT SELECTION

At the first stage of analysis, events with two or three charged particles originated from the interaction region, and at least four photons with energy greater than 20 MeV are selected. The total energy deposition in the calorimeter for these events is required to be greater than 300 MeV.

For selected events the vertex fit is performed using parameters of two charged tracks. The quality of the vertex fit is characterized by the parameter χ^2_r. If there are three charged tracks in an event, two of them with the lowest χ^2_r value are selected. The found vertex is used to refine the parameters of charged particles and photons. Then the kinematic fit to the $e^+e^- \to \pi^+\pi^-\pi^0\gamma\gamma$ hypothesis is performed with the requirement of energy and momentum balance and the π^0 mass constraint. The π^0 candidate is a two photon pair with invariant mass in the range $70 < m_{12} < 200$ MeV. The invariant mass of the second photon pair (η-meson candidate) must be in the range $400 < m_{34} < 700$ MeV. The quality of the kinematic fit is characterized by the parameter $\chi^2_{3\pi2\gamma}$. All possible combinations of photons are tested, and the combination with the smallest $\chi^2_{3\pi2\gamma}$ value is chosen. The photon parameters after the kinematic fit are used to recalculate the η-candidate invariant mass (M_η). The event is then refitted with η-mass constraint. The refined energy of the η-meson candidate is used to calculate the invariant mass of the system recoiling against η meson (M^{rec}_η).

Events of the process $e^+e^- \to \omega\eta$ are selected by the conditions $\chi^2_{3\pi2\gamma} < 30$ and $0.65 < M^{rec}_\eta < 0.9$ GeV. The main background source is the process $e^+e^- \to \pi^+\pi^-\pi^0\pi^0$. For its suppression, a kinematic fit to the hypothesis $e^+e^- \to \pi^+\pi^-\pi^0\pi^0(\gamma)$ is performed. In this fit, radiation of an additional photon along the beam axis is allowed. Events with $\chi^2_{4\pi(\gamma)} < 200$ are rejected.

The $\chi^2_{3\pi2\gamma}$ distribution for selected data events is shown in Fig. 1 in comparison with the simulated distributions for signal $e^+e^- \to \omega\eta$ and background $e^+e^- \to \pi^+\pi^-\pi^0\pi^0$ events.

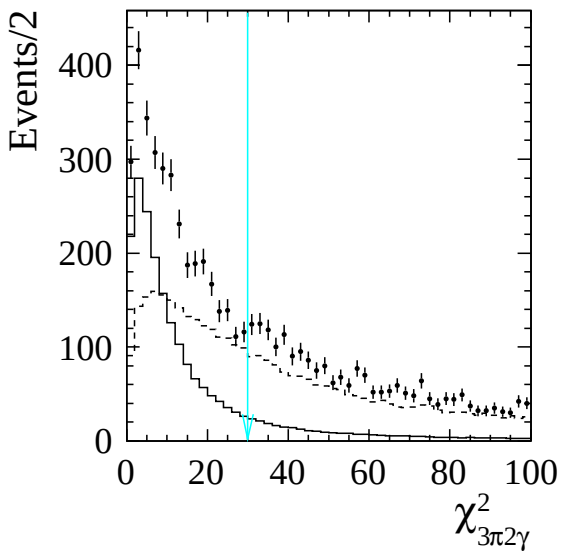

FIG. 1: The $\chi^2_{3\pi 2\gamma}$ distribution for selected data events (points with error bars). The solid and dashed histograms represent the shapes of signal $e^+e^- \to \omega\eta$ and background $e^+e^- \to \pi^+\pi^-\pi^0\pi^0$ distributions obtained using MC simulation, respectively. The arrow indicate the boundary of the condition $\chi^2_{3\pi 2\gamma} < 30$.

The narrow signal peak near zero is clearly seen in the distribution. However, the region $\chi^2_{3\pi 2\gamma} < 30$ contains a significant amount of background events.

V. DETERMINATION OF THE NUMBER OF SIGNAL EVENTS

The M_η spectrum for selected data events is shown in Fig. 2. It is seen that only about 25% of events contain an η meson. The spectrum is fitted with a sum of signal and background distributions. The background distribution is obtained using simulation of the process $e^+e^- \to \pi^+\pi^-\pi^0\pi^0$. A possible background simulation inaccuracy is taken into account by introducing a scale factor $\alpha_{4\pi}$. For energies below 1.594 GeV, the value of $\alpha_{4\pi}$ found in the fit is consistent with unity. At higher energies, there is significant background contribution from other processes, e.g., $e^+e^- \to \pi^+\pi^-\pi^0\pi^0\pi^0$. In this region $\alpha_{4\pi}$ is fixed to unity, and a linear function is added to describe contribution of other background processes. It is worth to note that in the energy region above 1.594 GeV the shape of the M_η distribution for $e^+e^- \to \pi^+\pi^-\pi^0\pi^0$ events is close to linear.

The signal distribution is described by a sum of three Gaussian distributions with param-

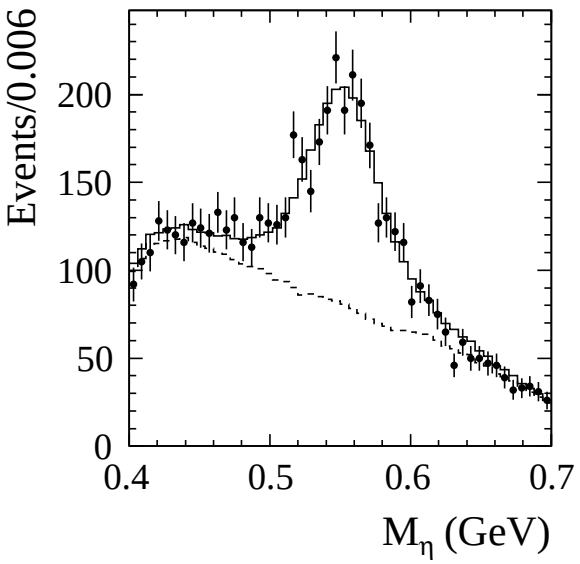

FIG. 2: The spectrum of the two-photon invariant mass of the η-meson candidate for selected data events (points with error bars). The solid histogram is the result of the fit to the data spectrum with a sum of signal and background distributions. The background contribution is shown by the dashed histogram.

eters determined from the fit to the M_η distributions for $e^+e^- \to \omega\eta \to \pi^+\pi^-\pi^0\eta$ simulated events. To account for a possible inaccuracy of the signal simulation, two parameters are introduced: mass shift ΔM_η and smearing parameter $\Delta\sigma_{M_\eta}$. The latter is quadratically added to all Gaussian sigmas. The parameters ΔM_η and $\Delta\sigma_{M_\eta}$ are determined from the fit to the M_η spectrum for events from the energy range $1.544 \leq E < 1.794$ GeV, where the signal-to-background ratio is maximal. The obtained values $\Delta M_\eta = -0.2 \pm 1.3$ MeV and $\Delta\sigma_{M_\eta} = 8.0 \pm 7.6$ MeV are consistent with zero. Therefore, these parameters are set to zero in the fit. Their errors are used to estimate systematic uncertainty in the fitted number of signal events due to a possible difference between data and simulation in the η-meson line shape. This uncertainty is found to be 1.6%.

To estimate the systematic uncertainty due to imperfect description of the shape of the background distribution, we perform the fit with an additional linear background as described above below 1.594 GeV, and without the linear background but with free $\alpha_{4\pi}$ above. The obtained systematic uncertainty is 5% below 1.594 GeV and 1.2% above.

The number of signal and background events obtained from the fit to the M_η spectrum in Fig. 2 are 1413±67 and 4123±88, respectively. The events with η meson belong to the process

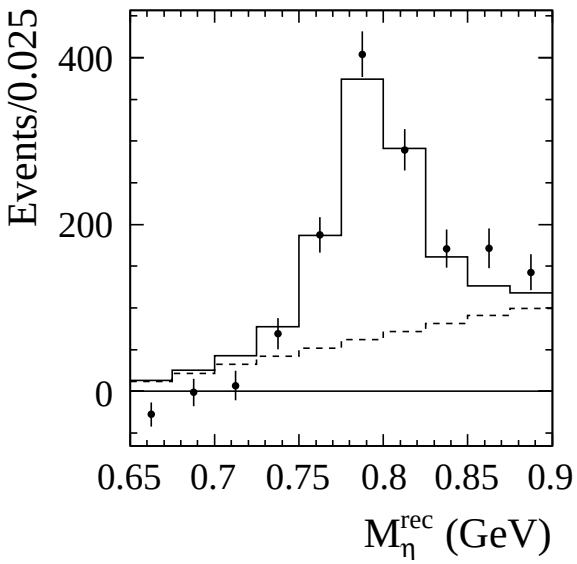

FIG. 3: The M_η^{rec} distribution for data $e^+e^- \to \pi^+\pi^-\pi^0\eta$ events (points with error bars). The solid histogram represents the result of the fit described in the text. The dashed histogram shows the fitted distribution for non-$\omega\eta$ events.

$e^+e^- \to \pi^+\pi^-\pi^0\eta$. To obtain number of $e^+e^- \to \omega\eta$ events, the M_η^{rec} spectrum is analyzed. We divide the interval $0.65 < M_\eta^{rec} < 0.9$ GeV into 10 subintervals. In each subinterval the number of events with η meson is determined from the fit to the M_η distribution. The results of these fits are shown in Fig. 3 as a M_η^{rec} histogram.

Such M_η^{rec} distributions are obtained for each c.m. energy interval listed in Table I. The M_η^{rec} distributions are fitted with a sum of the distribution for the process $e^+e^- \to \omega\eta$, which has a peak near the ω-meson mass, and a flat distribution for non-$\omega\eta$ events. To obtain the shape of the latter distribution, the $e^+e^- \to \pi^+\pi^-\pi^0\eta$ simulation with the uniform distribution of the final particle momenta over the phase space is used. Above 1.594 GeV, where the simulated distribution is close to linear, a linear function is used in the fit to describe the non-$\omega\eta$ background. It should be noted that the fitted numbers of background events are consisted with zero below 1.594 GeV.

Our preliminary analysis of intermediate states in the process $e^+e^- \to \pi^+\pi^-\pi^0\eta$ [13] shows that a significant contribution to the cross section comes from the $\rho a_0(980)$ intermediate state. Therefore, at energies above 1.594 GeV, the alternative background model $e^+e^- \to \rho a_0(980)$ is also tested. The difference between fit results for the two background models is used as an estimate of the systematic uncertainty. Below 1.594 GeV, where the

non-$\omega\eta$ background is small, the difference between fit results with nonzero and zero background is taken as an estimate of the systematic uncertainty associated with the shape of the non-$\omega\eta$ distribution.

The ω-meson line shape is described by a sum of three Gaussian distributions with parameters obtained from the fit to the the simulated signal M_η^{rec} distribution. To obtain corrections for the data-simulation difference in the mass scale and mass resolution, the parameters ΔM_ω and $\Delta\sigma_\omega$ are introduced. These parameters are determined from the fit to the total mass spectrum shown in Fig. 3. The $\Delta\sigma_\omega$ is found to be consistent with zero, while $\Delta M_\omega = 7.5 \pm 1.9$ MeV. The systematic uncertainty due to imperfect simulation the ω-meson line shape is estimated to be 1.4%. The total number of $e^+e^- \to \omega\eta$ events obtained from the fit to the M_η^{rec} distribution shown in Fig. 3 is 852 ± 69. The number of background events is 564 ± 80.

The obtained numbers of $e^+e^- \to \omega\eta$ events for different energy intervals are listed in Table I. The first error is statistical and the second is systematic, due to the background description in the fit to the M_η^{rec} distribution. The energy independent systematic uncertainty on the number of signal events is 5.4% below 1.594 GeV and 2.4% above.

VI. DETECTION EFFICIENCY

The detection efficiency for events of the process $e^+e^- \to \omega\eta \to \pi^+\pi^-\pi^0\eta$ is determined using MC simulation. As was discussed in Sec. II, the simulation takes into account radiative corrections. Therefore, the detection efficiency depends on the Born cross section used in simulation. For the process under study, the Born cross section measured in the work [3] is taken as a first approximation. Then the cross section is corrected taking into account our measurement, and the detection efficiency is recalculated. Then the third iteration is performed. The energy dependence of the detection efficiency obtained is shown in Fig. 4. The efficiency decrease above 1.7 GeV is explained by the steep falloff of the $e^+e^- \to \omega\eta$ cross section in this energy region and increase of the fraction of events with a hard photon radiated from the initial state. The difference between the detection efficiencies found after the second and third iterations is taken as an estimate of the model uncertainty. It is 1% below 1.694 GeV and 10% above.

Imperfect simulation of detector response leads to a difference between the actual detec-

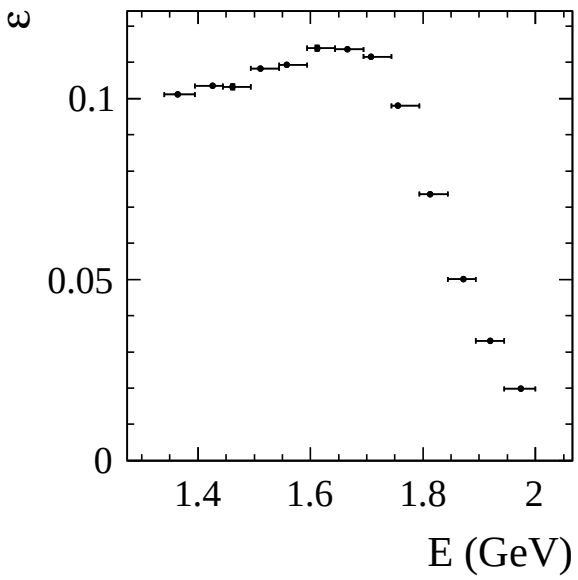

FIG. 4: The energy dependence of the detection efficiency for the process $e^+e^- \to \omega\eta \to \pi^+\pi^-\pi^0\eta$.

tion efficiency ε and the efficiency determined using MC simulation ε_{MC}:

$$\varepsilon = \varepsilon_{MC} \prod_{i=1}^{n} (1 + \delta_i), \tag{1}$$

where δ_i are the efficiency corrections for different effects. The main selection criterion for signal events is $\chi^2_{3\pi 2\gamma} < 30$. The quality of the simulation of the kinematic-fit χ^2 distribution is studied using events of the process $e^+e^- \to \omega\pi^0 \to \pi^+\pi^-\pi^0\pi^0$, which has a large cross section and the same number of the final particles as the process under study. Events from the energy range $1.394 \le E < 1.594$ GeV, where the $e^+e^- \to \omega\pi^0$ cross section is maximal, are selected using the preliminary conditions described in Sec. IV, and kinematically fitted to the $e^+e^- \to \pi^+\pi^-\pi^0\pi^0$ hypothesis. The efficiency correction is calculated as

$$\delta_1 = \frac{N'_{MC}/N_{MC}}{N'/N} - 1, \tag{2}$$

where N and N_{MC} are the numbers of signal events selected with the standard criteria in data and simulation, while N' and N'_{MC} are the numbers of events selected with a looser condition on the parameter under study. To determine the number of $e^+e^- \to \omega\pi^0$ events, the spectrum of the invariant mass recoiling against most energetic π^0 meson in an event, which has a peak at the ω-meson mass, is fitted. From the numbers of events in the ω peak obtained with the conditions $\chi^2_{4\pi} < 30$ and $\chi^2_{4\pi} < 200$, the correction value is found to be $\delta_1 = (2.5 \pm 1.1)\%$.

To determine the correction for the condition $\chi^2_{4\pi(\gamma)} > 200$, events from the energy region $1.594 \leq E < 1.744$ GeV selected with the tighter cuts $\chi^2_{3\pi 2\gamma} < 20$ and $0.76 < M_\eta^{rec} < 0.83$ GeV are used. The numbers of η-meson events with and without the condition on $\chi^2_{4\pi(\gamma)}$ are obtained from the fit to the M_η distribution. The correction is calculated to be $\delta_2 = (3.8 \pm 4.6)\%$.

The difference between data and simulation in photon conversion in detector material before the tracking system is studied using events of the process $e^+e^- \to \gamma\gamma$. The corresponding efficiency correction is $\delta_3 = (-1.35 \pm 0.05)\%$.

The largest part of the systematic uncertainties associated with data-MC simulation difference in track reconstruction cancels as a result of luminosity normalization. The difference in the track reconstruction for electrons and pions was studied in Ref. [15]. The corresponding correction $\delta_4 = (-0.3 \pm 0.2)\%$.

The total correction is $(4.7 \pm 4.7)\%$. The corrected values of the detection efficiency are listed in Table I. The statistical error of the efficiency is less than 1% and included to the statistical error of the measured cross section.

VII. THE BORN CROSS SECTION FOR $e^+e^- \to \omega\eta$

The experimental values of the $e^+e^- \to \omega\eta$ visible cross section are calculated as follows

$$\sigma_{vis,i} = \frac{N_i}{L_i \varepsilon_i B(\omega \to \pi^+\pi^-\pi^0)}, \tag{3}$$

where N_i, L_i, and ε_i are the number of selected data events, integrated luminosity, and detection efficiency for the i-th energy interval, and $B(\omega \to \pi^+\pi^-\pi^0)$ is the branching fraction for the $\omega \to \pi^+\pi^-\pi^0$ decay.

The visible cross section is related to the Born cross section (σ) by the following expression [9]:

$$\sigma_{vis}(E) = \int_0^{x_{max}} F(x,E)\sigma(E\sqrt{1-x})dx, \tag{4}$$

where the function $F(x,E)$ describes the probability of radiation of photons with total energy $xE/2$ by the initial electron and positron. The right side of Eq. (4) can be rewritten in the more conventional form:

$$\int_0^{x_{max}} F(x,E)\sigma(E\sqrt{1-x})dx = \sigma(E)(1+\delta(E)), \tag{5}$$

TABLE I: The c.m. energy interval, weighted average energy for the interval ($\overline{E}$), integrated luminosity (L), number of selected data events (N), detection efficiency (ε), radiative correction factor ($1+\delta$), measured Born cross section (σ). For N and σ, the statistical and energy dependent systematic errors are quoted. The energy independent uncertainty on the cross section is 7.5%, 5.8%, and 11.5% in the energy ranges $E < 1.594$ GeV, $1.594 \le E < 1.694$ GeV, $E \ge 1.694$ GeV, respectively.

Energy interval (GeV)	$\overline{E}$ (GeV)	L (nb^{-1})	N	ε (%)	$1+\delta$	σ (nb)
1.340–1.394	1.36	2082	$-10 \pm 7 \pm 0$	10.1	0.78	$-0.07 \pm 0.05 \pm 0$
1.394–1.444	1.43	2256	$32 \pm 11 \pm 0$	10.4	0.83	$0.19 \pm 0.06 \pm 0$
1.444–1.494	1.46	1095	$30 \pm 8 \pm 0$	10.3	0.85	$0.35 \pm 0.10 \pm 0$
1.494–1.544	1.51	2193	$28 \pm 18^{+36}_{-0}$	10.8	0.87	$0.15 \pm 0.10^{+0.19}_{-0}$
1.544–1.594	1.56	1024	$76 \pm 10 \pm 0$	10.9	0.87	$0.87 \pm 0.11 \pm 0.01$
1.594–1.644	1.61	1008	$111 \pm 19^{+4}_{-0}$	11.4	0.86	$1.26 \pm 0.21^{+0.05}_{-0.01}$
1.644–1.694	1.67	1854	$338 \pm 33^{+16}_{-0}$	11.4	0.89	$2.01 \pm 0.20^{+0.10}_{-0.03}$
1.694–1.744	1.71	1540	$140 \pm 27^{+23}_{-0}$	11.2	1.05	$0.87 \pm 0.18^{+0.15}_{-0.02}$
1.744–1.794	1.76	1722	$88 \pm 25^{+3}_{-0}$	9.8	1.31	$0.44 \pm 0.17^{+0.04}_{-0.03}$
1.794–1.844	1.81	2927	$55 \pm 25^{+2}_{-0}$	7.4	1.71	$0.17 \pm 0.14^{+0.03}_{-0.02}$
1.844–1.894	1.87	2678	$-7 \pm 19^{+4}_{-0}$	5.0	2.21	$-0.03 \pm 0.15^{+0.02}_{-0}$
1.894–1.944	1.92	3702	$-17 \pm 17^{+5}_{-0}$	3.3	2.29	$-0.06 \pm 0.14^{+0.03}_{-0.01}$
1.944–2.000	1.97	2930	$-11 \pm 8^{+2}_{-0}$	2.0	3.30	$-0.06 \pm 0.17^{+0.03}_{-0.01}$

where $\delta(E)$ is the radiative correction.

Experimental values of the Born cross section are determined as follows. The energy dependence of the measured visible cross section is fitted with Eq. (4), in which the Born cross section is given by a theoretical model describing data well. The model parameters obtained in the fit are used to calculate $\delta(\overline{E}_i)$, where $\overline{E}_i$ is the weighted average c.m. energy for i-th energy interval, defined in Sec. II. The values of the Born cross section are then obtained as $\sigma_i = \sigma_{vis,i}/(1+\delta(\overline{E}_i))$.

The Born cross section is described by a sum of two resonance contributions:

TABLE II: The obtained fit parameters.

$B_{\omega'} \times 10^7$	$0.16^{+0.09}_{-0.07}$
$B_{\omega''} \times 10^7$	4.4 ± 0.5
$M_{\omega''}$ (MeV)	1660 ± 10
$\Gamma_{\omega''}$ (MeV)	110 ± 20

$$\sigma(E) = \frac{12\pi}{E^3}\left|\sqrt{\frac{B_{\omega'}}{P_f(m_{\omega'})}}\frac{m_{\omega'}^{3/2}\Gamma_{\omega'}}{D_{\omega'}} - \sqrt{\frac{B_{\omega''}}{P_f(m_{\omega''})}}\frac{m_{\omega''}^{3/2}\Gamma_{\omega''}}{D_{\omega''}}\right|^2 P_f(E), \quad (6)$$

where $B_V = B(V \to e^+e^-)B(V \to \omega\eta)$ is the product of the branching fractions for the V decay to e^+e^- and $\omega\eta$, $D_V = E^2 - m_V^2 + iE\Gamma_V$, m_V and Γ_V are the mass and width of the resonance V ($V = \omega'$ or ω''). The phase space factor $P_f(E)$ is given by

$$P_f(E) = q(E)^3,\ q(E) = \frac{1}{2E}\sqrt{(E^2 - (m_\omega - m_\eta)^2)(E^2 - (m_\omega + m_\eta)^2)}. \quad (7)$$

The first term in Eq. (6) describes the $\omega(1420)$ contribution. The second term is a sum of contributions of the $\omega(1650)$ and $\phi(1680)$ resonances. The phase between the first and second terms is chosen to be equal to π (see discussion below).

The free fit parameters are $B_{\omega'}, B_{\omega''}, m_{\omega''}, \Gamma_{\omega''}$. The mass and width of the $\omega(1420)$ resonance are fixed at their Particle Data Group (PDG) values [14]. In the fit negative numbers of events (see Table I) are substituted by zero values. The fitted parameters are listed in Table II. The fit yields $\chi^2 = 14.5$ for 9 degrees of freedom. The fitted curve together with obtained values of the Born cross section is shown in Fig. 5. The fit performed with zero phase between the ω' and ω'' amplitudes provides a significantly worse ($\chi^2 = 41.6$) description of the cross-section data.

The fitted ω'' mass is in agreement with the PDG mass of both $\omega(1650)$ and $\phi(1680)$ resonances [14], while the fitted width is smaller than the PDG estimate for the $\omega(1650)$ width, 315 ± 35 MeV [14], but agrees with the PDG value, 150 ± 50 MeV [14], for the $\phi(1680)$ resonance. The contribution of the $\omega(1420)$ is small compared with that of the ω''. However, this contribution is necessary to describe the asymmetry of the peak in the measured cross section. The asymmetry is explained by constructive interference of the ω' and ω'' amplitudes on the left side of the peak and destructive interference on the right side.

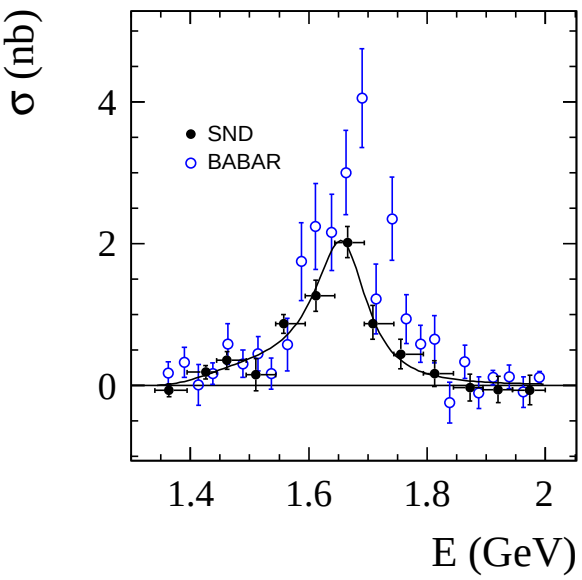

FIG. 5: The $e^+e^- \to \omega\eta$ cross section measured in this work (filled circles) and in the BABAR experiment [3] (open circles). The curve is the result of the fit described in the text. The errors of the SND data are statistical and systematic, combined in quadrature.

The numerical values of the measured Born cross section and radiative correction are listed in Table I. The quoted errors of the cross section are statistical and energy dependent systematic. The latter includes the energy dependent systematic uncertainty on the number of events and the model uncertainty of the radiative correction, which is estimated by varying the fitted parameters within their errors. The sources of the energy independent systematic uncertainty are listed in Table III. This uncertainty is equal to 7.5%, 5.8%, and 11.5% in the energy ranges $E < 1.594$ GeV, $1.594 \le E < 1.694$ GeV, $E \ge 1.694$ GeV, respectively.

The comparison of our cross section data with the previous BABAR measurement [3] is shown in Fig. 5. Our results have better accuracy and disagree with the BABAR data at $E > 1.6$ GeV.

VIII. SUMMARY

In this paper we have analyzed data collected with the SND detector at the VEPP-2000 e^+e^- collider. In the $\pi^+\pi^-\pi^0\eta$ final state we have selected about 850 $\omega\eta$ events and have measured the $e^+e^- \to \omega\eta$ cross section in the c.m. energy range 1.34–2.00 GeV. The obtained cross section data are the most accurate to date. Above 1.6 GeV they disagree

TABLE III: The systematic uncertainties on the measured cross section.

Source	Value (%)
Luminosity	2
Uncertainties on ΔM_η, $\Delta\sigma_{M_\eta}$	1.6
Background shape in the M_η distribution	5.0 at $E < 1.594$ GeV
	1.2 at $E \geq 1.594$ GeV
Uncertainty on ΔM_ω	1.4
Model uncertainty of the detection efficiency	1 at $E < 1.694$ GeV
	10 at $E \geq 1.694$ GeV
Condition on $\chi^2_{3\pi 2\gamma}$	1.1
Condition on $\chi^2_{4\pi}$	4.6
Photon conversion	0.05
Charged track reconstruction	0.2
Total	7.5 at $E < 1.594$ GeV
	5.8 at $1.594 \leq E < 1.694$ GeV
	11.5 at $E \geq 1.694$ GeV

with previous BABAR measurements [3]. The measured cross section is well fitted by a sum of two resonance contributions, from the $\omega(1420)$ and from an effective resonance describing the $\omega(1650)$ and $\phi(1680)$ contributions. The fitted $\omega(1420)$ amplitude is small, but necessary to describe the asymmetry of the peak in the measured cross section.

IX. ACKNOWLEDGMENTS

Part of this work related to the photon reconstruction algorithm in the electromagnetic calorimeter is supported by the Russian Science Foundation (project No. 14-50-00080).

[1] M. N. Achasov *et al.*, Nucl. Instrum. Methods Phys. Res., Sect. A 598, 31 (2009); V. M. Aulchenko *et al.*, ibid. 598, 102 (2009); A. Yu. Barnyakov *et al.*, ibid. 598, 163 (2009); V. M. Aulchenko *et al.*, ibid. 598, 340 (2009).

[2] Yu. M. Shatunov *et al.*, in Proceedings of the 7th European Particle Accelerator Conference, Vienna, 2000, p. 439, http://accelconf.web.cern.ch/AccelConf/e00/PAPERS/MOP4A08.pdf.

[3] B. Aubert *et al.* (BABAR Collaboration), Phys. Rev. D**73**, 052003 (2006).

[4] B. Aubert *et al.* (BaBar Collaboration), Phys. Rev. D **76**, 092005 (2007).

[5] B. Aubert *et al.* (BaBar Collaboration), Phys. Rev. D **77**, 092002 (2008).

[6] E. V. Abakumova *et al.*, Nucl. Instrum. Meth. A **744**, 35 (2014).

[7] E. V. Abakumova, M. N. Achasov, A. A. Krasnov, N. Y. Muchnoi and E. E. Pyata, JINST **10**, No. 09, T09001 (2015)

[8] D. N. Shemyakin *et al.* (CMD-3 Collaboration), Phys. Lett. B **756**, 153 (2016).

[9] E. A. Kuraev and V. S. Fadin, Yad. Fiz. **41**, 733 (1985) [Sov. J. Nucl. Phys. **41**, 466 (1985)].

[10] G. Bonneau and F. Martin, Nucl. Phys. B **27**, 381 (1971).

[11] S. Agostinelli **et al.**, Nucl. Instrum. Methods Phys. Res., Sect. A **506**, 250 (2003).

[12] S. Jadach, W. Placzek and B. F. L. Ward, Phys. Lett. B **390**, 298 (1997).

[13] V. P. Druzhinin *et al.* (SND Collaboration), in Proceeding of the 14th International Workshop on Meson Production, Properties and Interaction (MESON2016) Krakow, Poland, June 2016 (to be published).

[14] K. A. Olive *et al.* (Particle Data Group), Chin. Phys. C, **38**, 090001 (2014).

[15] M. N. Achasov *et al.* (SND Collaboration), JETP **101**, 1053 (2005).